THE JOURNAL OF PHYSICAL CHEMISTRY A
A JOURNAL OF THE AMERICAN CHEMICAL SOCIETY

Open Access
This article is licensed under CC-BY 4.0

pubs.acs.org/JPCA
Article

Resonant Photoionization of CO_2 up to the Fourth Ionization Threshold

Published as part of The Journal of Physical Chemistry A virtual special issue "Attosecond Chemistry".

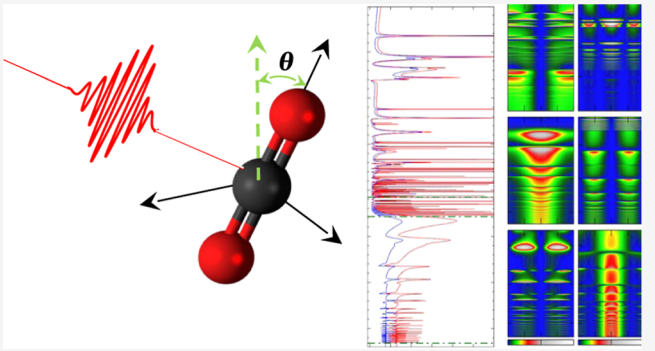
Prateek Pranjal, Jesús González-Vázquez, Roger Y. Bello,* and Fernando Martín

Cite This: *J. Phys. Chem. A* 2024, 128, 182−190

Read Online

ACCESS | Metrics & More | Article Recommendations

ABSTRACT: We present a comprehensive theoretical study of valence-shell photoionization of the CO_2 molecule by using the XCHEM methodology. This method makes use of a fully correlated molecular electronic continuum at a level comparable to that provided by state-of-the-art quantum chemistry packages in bound-state calculations. The calculated total and angularly resolved photoionization cross sections are presented and discussed, with particular emphasis on the series of autoionizing resonances that appear between the first and the fourth ionization thresholds. Ten series of Rydberg autoionizing states are identified, including some not previously reported in the literature, and their energy positions and widths are provided. This is relevant in the context of ongoing experimental and theoretical efforts aimed at observing in real-time (attosecond time scale) the autoionization dynamics in molecules.



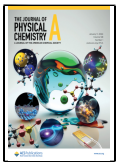
INTRODUCTION

The development of attosecond VUV/XUV pulses has opened new doorways for imaging and steering electron dynamics in many-electron systems, in particular, molecular systems.[1−12] Recent examples also include retrieving real-space movies of the internal motion in molecules,[13,14] monitoring the birth of a photoelectron in helium,[15] extracting photoionization time delays of molecules in the vicinity of shape and Feshbach resonances,[8,10,16−19] and the observation of correlation-driven charge migration in a DNA building block.[11] The use of these light sources usually leads to ionization, where in addition to the photoelectron ejection, other processes involving two or more electrons can also take place, e.g., autoionization of Feshbach resonances, ionization leaving the remaining ion in an excited state (shakeup), inner-shell ionization followed by Auger decay, and Auger decay combined with shakeup. Thus, any comprehensive theoretical description of these types of experiments requires a fully correlated treatment of the electronic continuum. In addition, photoionization processes of many-electron systems are also sensitive to interchannel couplings, including those between energetically open and closed channels.

All of the above has prompted the development of advanced theoretical methods based on different approximations to account for electron correlation in the molecular continuum. Among these methods, the multichannel Schwinger configuration interaction method (MCCI),[20−22] the variational Complex-Khon[23,24] method, the UK Molecular R-matrix,[25] and the XCHEM method[26,27] are well established nowadays. In particular, the XCHEM approach combines standard quantum chemistry techniques with a single-center hybrid Gaussian-B-spline basis (GABS),[26] providing a fully correlated description of the electronic continuum at a level similar to that provided by quantum chemistry packages in bound state calculations. This makes XCHEM particularly well suited to study photoionization processes in many-electron systems. In previous works, XCHEM has been shown to provide accurate photoionization spectra in the resonance regions of He, Ne, and Ar atoms,[27−29] and small molecules such as N_2, O_2, and more recently H_2O.[30−33]

In the present paper, we take advantage of the XCHEM capabilities to study valence-shell one-photon single ionization of the CO_2 molecule, for photon energies between the first and fourth ionization thresholds. While the energy region above the fourth ionization threshold has been extensively studied, both theoretically and experimentally,[34−42] the existing theoretical

Received: October 20, 2023
Revised: November 28, 2023
Accepted: November 29, 2023
Published: December 20, 2023



Downloaded via UNIV AUTONOMA DE MADRID on February 9, 2024 at 11:14:59 (UTC).
See https://pubs.acs.org/sharingguidelines for options on how to legitimately share published articles.

ACS Publications
© 2023 American Chemical Society

https://doi.org/10.1021/acs.jpca.3c06947
J. Phys. Chem. A 2024, 128, 182−190

information for energies below this threshold is rather scarce. This is because, despite its apparent simplicity, the CO_2 molecule presents very rich and complex photoionization dynamics. As schematically depicted in Figure 1, the removal

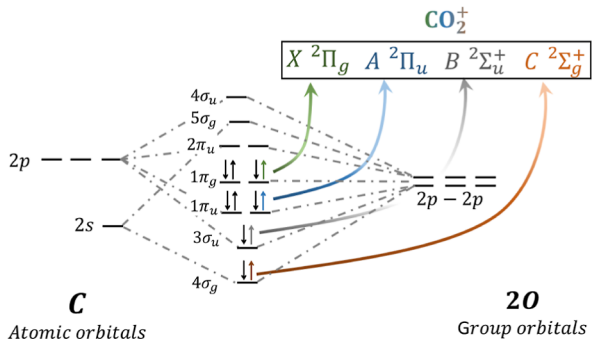


Figure 1. Schematic representation of the molecular orbitals of CO_2 and the cationic electronic states resulting from the removal of an electron from different molecular orbitals.

of an electron from the $1\pi_g$ (HOMO), $1\pi_u$ (HOMO − 1), $3\sigma_u$ (HOMO − 2), and $4\sigma_g$ (HOMO − 3) molecular orbitals leaves the remaining CO_2^+ cation in the $X^2\Pi_g$, $A^2\Pi_u$, $B^2\Sigma_u^+$, or $C^2\Sigma_g^+$ electronic states lying at 13.778, 17.314, 18.077, and 19.394 eV, respectively.[43] The fourth excited state of the $CO_2^+(C^2\Sigma_g^+)$ cation lies just 6 eV above the energy of the CO_2^+ $(X^2\Pi_g)$ ground state. Consequently, several series of Rydberg autoionizing states converging to the different ionization thresholds are expected to overlap in this energy region. Total single-photon ionization cross sections in this energy region have been previously measured in photoabsorption experiments using synchrotron radiation sources.[44−50] In these experiments, several series have been identified, namely, the so-called Tanaka−Ogawa, Lindholm, Henning sharp and diffuse, "absorption", "apparent emission", and "weak absorption" series. However, their assignment and characterization remain uncertain. In addition, most of these resonances have not been theoretically described so far.

In this work, we have evaluated one-photon single-ionization fully differential cross sections and analyzed the effect of the autoionizing Rydberg states lying below the fourth ionization threshold. We have identified several series of Rydberg states, including some not observed in the existing experiments, e.g., the $1\pi_u^{-1}nd\pi_g$ and $1\pi_u^{-1}ns\sigma_g$ series converging to the second ionization threshold, as well as the $3\sigma_u^{-1}nd\pi_g$ and $4\sigma_g^{-1}nf\pi_u$ series converging to the third and fourth ionization thresholds, respectively. The members of the different Rydberg series have been characterized and, in most cases, their corresponding energy positions and widths are given. Finally, the fully differential cross sections for photon energies above the fourth ionization thresholds are provided and compared with experimental and theoretical results found in the literature. The good agreement found at these higher energies gives additional support to our predictions at lower energies.

METHODS AND COMPUTATIONAL DETAILS

One-photon ionization cross sections, molecular-frame photoelectron angular distributions (MFPADs), and β asymmetry parameters were calculated at a fixed internuclear distance of R = 2.1943 au using the XCHEM methodology.[27] This methodology has been explained in detail elsewhere,[26,27,30−32] so only the computational details will be given here.

The initial set of orbitals used in the XCHEM calculations are the CO_2^+ $(X^2\Pi_g)$ ground-state natural orbitals. The cationic ground state was obtained from a complete active space configuration interaction (CAS-CI) calculation, where the active space included the first five σ_g, three σ_u, two π_u, and one π_g orbitals with the $1-2\sigma_g$ and $1\sigma_u$ core orbitals always doubly occupied (see Figure 1). These orbitals were optimized using a restricted active space SCF (SA-RASSCF) calculation using MOLCAS[51] where they form the active space and in which only the CO_2^+ $(X^2\Pi_g)$ ground state was included in the state average. The one-electron basis was aug-cc-pVTZ.[52] The neutral ground state was computed by constructing the $(N + 1)$-electron configuration state functions (CSFs) using the same orbitals as in the MOLCAS calculations of the cation target state. In the close-coupling calculation, the four lowest channels, $X^2\Pi_g$, $A^2\Pi_u$, $B^2\Sigma_u^+$, and $C^2\Sigma_g^+$, were included. We note that a similar active space was used in a previous work,[42] obtaining ionization potentials in very good agreement with the experimental values (see Table 1).

Table 1. Target Energies Absolute and Relative to the CO_2^+ Ground State[a]

state	XCHEM (eV)	UKRMol (eV)	experiment (eV)
$X^2\Pi_g$	0.00 (13.51)	0.00 (14.85)	0.0 (13.80)
$A^2\Pi_u$	4.08 (17.59)	3.97 (18.82)	3.8 (17.60)
$B^2\Sigma_u^+$	4.29 (17.80)	4.45 (19.27)	4.3 (18.10)
$C^2\Sigma_g^+$	5.66 (19.17)	5.77 (20.59)	5.6 (19.40)

[a]The present results are compared to the UKRMol results, obtained using the same active space[42,53] and the experimental values.[54]

The set of monocentric GABS basis functions[26] used to describe the photoelectron is placed at the system origin, with the B-splines being nonzero for radii $r > R_0$ and the monocentric Gaussian being nonzero for a radii $r < R_1$ such that $R_0 \leq R_1$. The B-splines part of the basis consists of a set of 800 B-splines of order $k = 7$ extending from $R_0 = 8$ au up to $R_{max} = 400$ a_0 with $l \leq 7$. The Gaussian part contains a set of 22 even tempered functions $G_i^M(r) \propto r^{2\zeta+l}\, e^{-\alpha_i r^2}$, with $\alpha_i = \alpha_0\beta^i$ ($\alpha_0 = 0.01$, $\beta = 1.46$, $i = 0, 1, ..., 21$), and $\zeta = 0$, $l \leq 7$.

In this work, our focus has been on the energy region between the first $(X^2\Pi_g)$ and fourth $(C^2\Sigma_g^+)$ ionization thresholds. Since only four channels have been included in the close-coupling calculation, no autoionizing resonances are expected to be present beyond the fourth $(C^2\Sigma_g^+)$ ionization threshold. No energy shift has been applied to the data, hence, the positions of the resonance peaks are slightly shifted to lower photon energies when compared to experimental results.[43]

Resonance Analysis. The energy positions and widths of the Rydberg autoionizing states have been calculated from the photoionization spectra. The total phase of the scattering states was fitted to the analytical expression[55] in eq 1, which describes the behavior of the scattering phase in the vicinity of an autoionizing state

$$\delta(E) = \delta_0(E) + \tan^{-1}\frac{\Gamma_n}{2(E - E_n)} \quad (1)$$

where δ_0 is a smoothly varying background, and E_n and Γ_n are the resonance position and width, respectively. The resonances have to be isolated to be able to employ this equation. Thus, in

https://doi.org/10.1021/acs.jpca.3c06947
J. Phys. Chem. A 2024, 128, 182−190

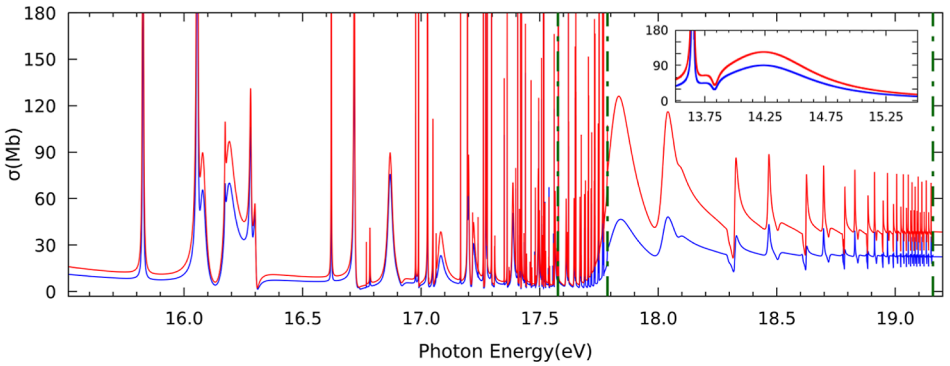


Figure 2. Computed total photoionization cross sections of CO_2 as a function of the photon energy. The comparison between length (red solid line) and velocity (blue solid line) gauges is also depicted. Green dashed line: energy position of each ionization threshold.

case of partially overlapping resonances, only an estimate of the resonance position and width can be given.

The autoionizing states have been assigned to different Rydberg series considering the available literature and using the Rydberg equation

$$E_0 = \mathrm{IP} - \frac{R}{(n-\delta)^2} \tag{2}$$

where E_0 is the resonance position, IP is the ionization potential of the state, R is the Rydberg constant, n is the principal quantum number of the Rydberg electron, and δ is the quantum defect. The quantum defect δ correlates with the orbital angular momentum l. Larger values ($\delta \sim 1$) are expected for $l = 0$, while small values ($\delta \sim 0$) are expected for $l = 2, 3$.

RESULTS AND DISCUSSIONS

Photoionization at Low Photoelectron Energies. Figure 2 depicts the total photoionization cross section for one-photon absorption for photon energies between the first and fourth ionization thresholds. The cross sections calculated in length and velocity gauges are generally in good agreement, reflecting the quality of the used basis set. As observed, the cross section is characterized by several autoionizing states. As no shift in energy has been applied to the data, the positions of the autoionizing Rydberg states might appear slightly shifted in photon energy when compared to experimental results. In the following, further consideration is dedicated to the characterization and assignment of these autoionizing Rydberg states.

Figures 3a and 4a present the partial photoionization cross section from the ground state leading to states of $^1\Sigma_u^+$ symmetry between the first and second, and between second and third ionization thresholds, respectively. The cross section between the second and third ionization thresholds (Figure 4a) is characterized by several autoionizing states associated with the Henning sharp $3\sigma_u^{-1}nd\sigma_g$ and diffuse $3\sigma_u^{-1}ns\sigma_g$ series converging to the third ionization threshold $B^2\Sigma_u^+$.[44−49] All Rydberg series identified are summarized in Tables 2−4, where the estimated energy positions and autoionization widths using eq 2 along with the value of δ characterizing the quantum defect are also presented. As observed, a quantum defect around $\delta = -0.127$ and $\delta = 1.167$ have been obtained for the Henning sharp and diffuse series, respectively. These values are in good agreement with those reported in refs 48 and 49, thus confirming the assignment. The spectrum between the first and second ionization thresholds (Figure 3a) appears to be dominated by three different series of autoionizing Rydberg

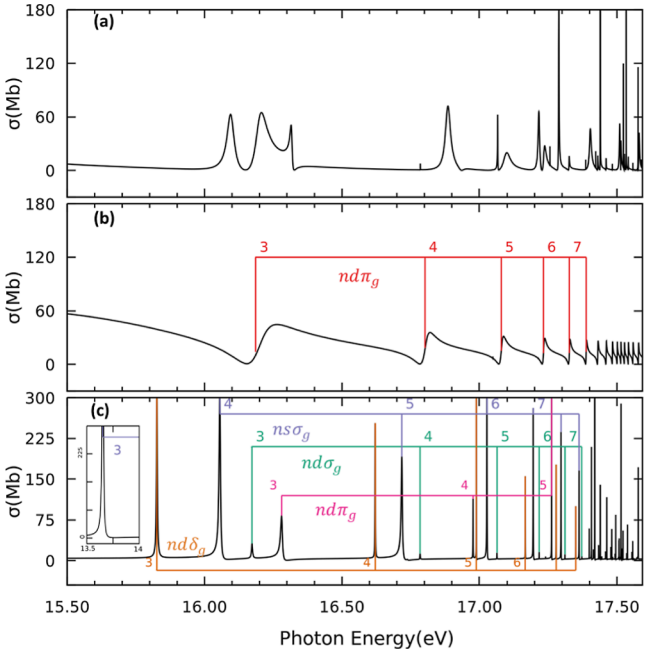


Figure 3. Partial photoionization cross sections for photon energies between the first ($X^2\Pi_g$) and second ($A^2\Pi_u$) ionization thresholds. (a) Molecular axis is placed parallel to the light polarization vector, i.e., $^1\Sigma_u^+$ final symmetry. (b) Model calculation limiting the number of channels included in the close coupling to the first two ionization thresholds for the $^1\Sigma_u^+$ final symmetry. (c) Molecular axis is placed perpendicular to the light polarization vector, i.e., $^1\Pi_u$ final symmetry. The corresponding resonances are indicated with nl labels.

states. Based on the analysis of Figure 4a, we see that some resonances correlate to low energy members of the Henning sharp and diffuse series. In order to further characterize this energy region, we performed additional calculations limiting the number of channels included in the close coupling to the first two ionization thresholds. Thus, in this scenario, resonances converging to higher ionization thresholds are not expected to appear in the spectrum. The result of these calculations is presented in Figure 3b. As observed, the cross section indeed features just a single Rydberg series, identified as $1\pi_u^{-1}nd\pi_g$ series converging to the second ionization threshold $A^2\Pi_u$. The lower members of the series exhibit broad Fano profiles with widths up to ∼100 meV (see Table 2). Therefore, the members of the $1\pi_u^{-1}nd\pi_g$ and the Henning sharp and diffuse series overlap in energy, making the full

https://doi.org/10.1021/acs.jpca.3c06947
J. Phys. Chem. A 2024, 128, 182−190

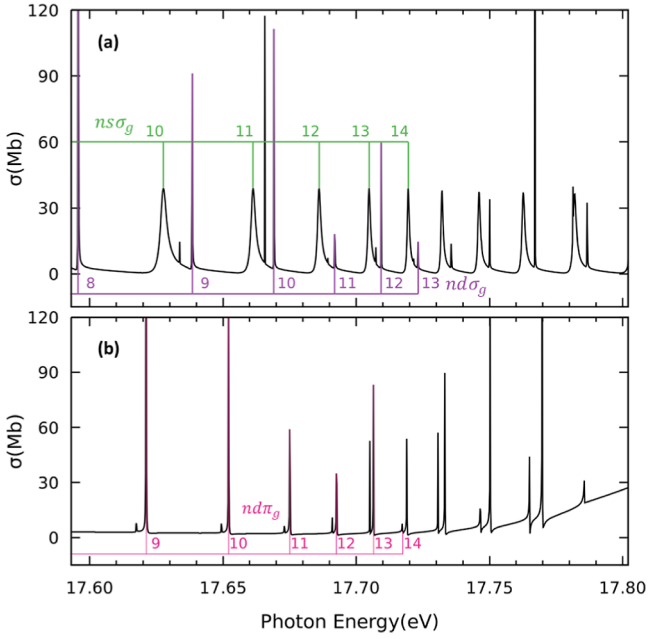


Figure 4. Same as Figure 3, but for photon energies between the second ($A^2\Pi_u$) and third ($B^2\Sigma_u^+$) ionization thresholds. (a) Molecular axis is placed parallel to the light polarization vector. (b) Molecular axis is placed perpendicular to the light polarization vector.

Table 2. $nd\pi_g$, $nd\sigma_g$, $nd\delta_g$, and $ns\sigma_g$ Rydberg Series Converging to the Second CO_2^+ ($A^2\Pi_u$) Ionic State[a]

n	calculated E (eV)	estimated E. (eV)	width Γ (meV)
	$nd\pi_g\ ^1\Sigma_u^+$	δ = 0.159	
3	16.1860	16.2296	100.49
4	16.8015	16.8065	31.41
5	17.0791	17.0819	15.15
6	17.2328	17.2344	8.46
7	17.3267	17.3276	5.23
	$nd(\sigma_g\ or\ \delta_g)^1\Pi_u$	δ =−0.151	
3	16.1729	16.2065	5.55
4	16.7836	16.7871	1.85
5	17.0630	17.0640	
6	17.2171	17.2171	
7	17.3109	17.3107	
	$nd(\sigma_g\ or\ \delta_g)^1\Pi_u$	δ = 0.241	
3	15.8260	15.7889	3.86
4	16.6203	16.6137	1.31
5	16.9807	16.9759	
6	17.1664	17.1665	
7	17.2787	17.2789	
	$ns\sigma_g\ ^1\Pi_u$	δ = 1.031	
3	13.6529	14.0668	11.60
4	16.0534	16.0331	6.09
5	16.7142	16.7130	5.27
6	17.0269	17.0257	1.04
7	17.1947	17.1948	

[a]The final symmetry is specified in each case. The corresponding resonances are indicated with nl labels in Figure 3. The estimated energies were obtained using eq 2 and the value of the quantum defect δ. The calculated energy positions and widths were obtained by fitting the corresponding scattering phase to eq 1.

characterization of Rydberg states in this energy region unfeasible.

Table 3. Same as Table 2, for $ns\sigma_g$, $nd\sigma_g$, and $nd\pi_g$ Rydberg Series Converging to the Third CO_2^+ ($B^2\Sigma_u^+$) Ionic State[a]

n	calculated E (eV)	estimated E (eV)	width Γ (meV)
	$ns\sigma_g\ ^1\Sigma_u^+$	δ = 1.167	
4		16.1065	
5		16.8759	
6		17.2195	
7		17.4021	
8		17.5106	
9		17.5803	
10	17.6274	17.6277	2.81
11	17.6611	17.6613	2.03
12	17.6859	17.6861	1.52
	$nd\sigma_g\ ^1\Sigma_u^+$	δ =−0.127	
3		16.4108	
4		17.0033	
5		17.2845	
6		17.4396	
7		17.5342	
8	17.5979	17.5961	
9	17.6415	17.6387	
10	17.6681	17.6694	
	$nd\pi_g{}^1\Pi_u$	δ =−0.094	
3	16.2663	16.3648	8.34
4	13.6931	16.9741	
5	17.2624	17.2615	
6	17.4194	17.4194	
7	17.5164	17.5154	

[a]The corresponding resonances are indicated with nl labels in Figures 3 and 4.

Table 4. Same as Table 2, for $np\sigma_u$, $nf\sigma_u$, $np\pi_u$, and $nf\pi_u$ Rydberg Series Converging to the Fourth CO_2^+ ($C^2\Sigma_g^+$) Ionic State[a]

n	calculated E. (eV)	estimated E. (eV)	width Γ (meV)
	$np\sigma_u\ ^1\Sigma_u^+$	δ = 0.443	
4	18.1021	18.0994	34.73
5	18.4679	18.5199	18.10
6	18.7361	18.7345	9.84
7	18.8597	18.8587	5.98
8	18.9377	18.9370	3.88
	$nf\sigma_u\ ^1\Sigma_u^+$	δ = 0.024	
4	18.3099	18.3146	12.15
5	18.6261	18.6257	6.49
6	18.7970	18.7943	4.51
7	18.8955	18.8957	3.12
8	18.9612	18.9614	2.04
	$np\pi_u{}^1\Pi_u$	δ = 0.568	
4	17.9971	18.0040	13.56
5	18.4486	18.4664	10.31
6	18.6973	18.6979	5.00
7	18.8298	18.8301	2.80
8	18.9124	18.9126	1.74
	$nf\pi_u{}^1\Pi_u$	δ =−0.038	
4	18.3126	18.3244	1.08
5	18.6174	18.6228	
6	18.7827	18.7857	
7	18.8823	18.8842	
8	18.9471	18.9483	

[a]The corresponding resonances are indicated with nl labels in Figure 5.

https://doi.org/10.1021/acs.jpca.3c06947
J. Phys. Chem. A 2024, 128, 182−190

Figure 3c shows the partial photoionization cross section from the ground state leading to states of $^1\Pi_u$ symmetry between the first and second ionization thresholds. The cross section features four different Rydberg series. Three of them, identified as $1\pi_u^{-1}ns\sigma_g$, $1\pi_u^{-1}nd\delta_g$, and $1\pi_u^{-1}nd\sigma_g$, are found to converge to the second ionization threshold $A^2\Pi_u$. In particular, the $1\pi_u^{-1}ns\sigma_g$ series characterized by a quantum defect of δ = 1.031, is assigned to the Tanaka−Ogawa series.[45−49] The assignment is made based on the value of quantum defect and the fact that the n = 3 member appears at 13.65 eV, very close to the ionization threshold (see insets in Figures 2 and 3c). As observed, the $1\pi_u^{-1}nd\sigma_g$ series presents very low cross sections compared to those of the $1\pi_u^{-1}nd\delta_g$ and $1\pi_u^{-1}ns\sigma_g$, and should not be visible experimentally. Taking this into account, we tentatively assign the $1\pi_u^{-1}nd\delta_g$ series to the Lindholm series.[45−49] The $3\sigma_u^{-1}nd\pi_g$ series converging to the third ionization threshold $B^2\Sigma_u^+$, has not been observed experimentally. Higher energy members of this series can be observed in Figure 4b, which depicts the partial cross section from the ground state leading to states of $^1\Pi_u$ symmetry between the second and third ionization thresholds.

Figure 5a,b shows the partial photoionization cross section between the third and fourth ionization thresholds from the ground state leading to states of $^1\Sigma_u^+$ and $^1\Pi_u$ symmetries, respectively. While the cross section exhibits four different Rydberg series converging to the fourth ionization threshold $C^2\Sigma_g^+$, just three have been observed experimentally in this energy region.[45,48,49] Two of them, the "absorption" and "apparent emission" series are identified as the $4\sigma_g^{-1}np\pi_u$ and $4\sigma_g^{-1}np\sigma_u$ series, respectively. In contrast, the "weak absorption" series assignment is still under debate. The members of the $4\sigma_g^{-1}nf\sigma_u$ series are generally broader than those of the $4\sigma_g^{-1}nf\pi_u$, and thus, more prone to be observed in experimental photoionization spectra. Based on this analysis, we tentatively assign the $4\sigma_g^{-1}nf\sigma_u$ series as the "weak absorption" series. There is an additional broad peak, labeled as "X" in Figure 5b, lying just at the ionization threshold (see Figure 2), making its assignment and further characterization unfeasible.

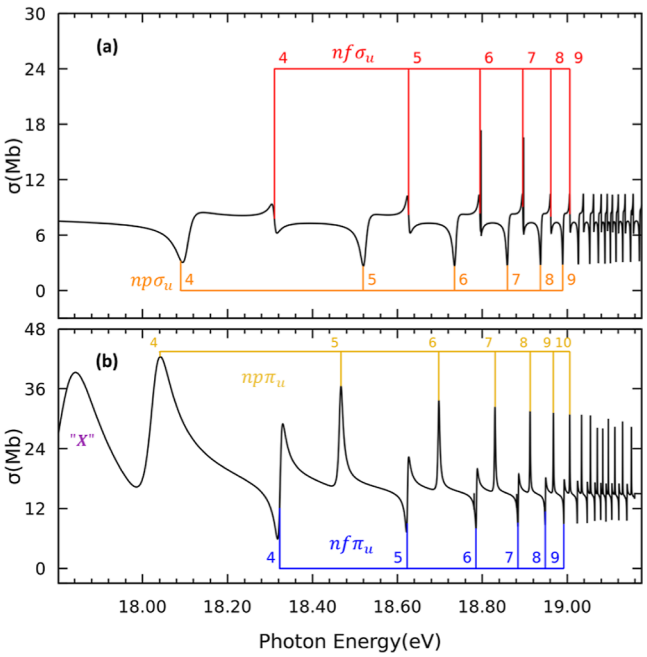


Figure 5. Same as Figure 3, but for photon energies between the third ($B^2\Sigma_u^+$) and fourth ($C^2\Sigma_u^+$) ionization thresholds. (a) Molecular axis is placed parallel to the light polarization vector. (b) Molecular axis is placed perpendicular to the light polarization vector.

We note that previous photoabsorption experiments in CO_2[44,45,56] have pointed out the existence of rather long vibrational progressions associated with the different series of Rydberg states. However, such vibrational progressions are difficult to resolve in the corresponding photoionization spectra.[43,47,50,56] This is probably due to (i) the limited energy resolution in photoionization experiments compared to photoabsorption experiments, (ii) the overlap between different vibrational progressions, and (iii) the fact that most of these resonances are long-lived so that their signature is ultimately washed out by nuclear motion. In contrast, our fixed-nuclei calculations allow for a more straightforward assignment of the resonance series. In addition, comparison with photoionization experiments with low energy resolution should be more straightforward.

Figure 6a,b presents the calculated energy positions for the different Rydberg series as a function of the effective quantum number $n^* = n - \delta$ for the $^1\Sigma_u^+$ and $^1\Pi_u$ final symmetries, respectively. A nearly perfect $(n^*)^{-2}$ scaling is observed in agreement with eq 2, thus confirming the validity of the assignment. For the higher n^*, the density of resonances increases significantly, so the assignment could be misleading. As expected, the autoionization widths decrease with the effective quantum number n^*. Some of the resonances observed in the photoionization cross sections are particularly narrow, with widths Γ < 10 meV, especially just below the different ionization thresholds. Therefore, in Tables 2−4 and in Figure 6a,b, only Rydberg states with widths $\Gamma \geq 1$ meV are shown. Such sharp resonances are usually not observed experimentally due to both the spectral resolution and the effect of the nuclear degrees of freedom (not considered in

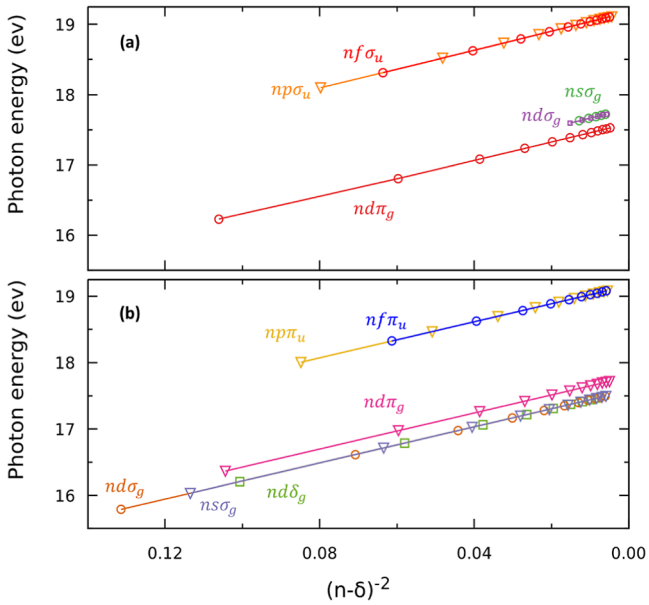


Figure 6. Energies of the different Rydberg series identified in the computed photoionization cross section as a function of $(n - \delta)^{-2}$. (a) Light polarization vector parallel to the molecular axis, i.e., $^1\Sigma_u^+$ final symmetry. (b) Light polarization vector perpendicular to the molecular axis, i.e., $^1\Pi_u$ final symmetry.

https://doi.org/10.1021/acs.jpca.3c06947
J. Phys. Chem. A 2024, 128, 182−190

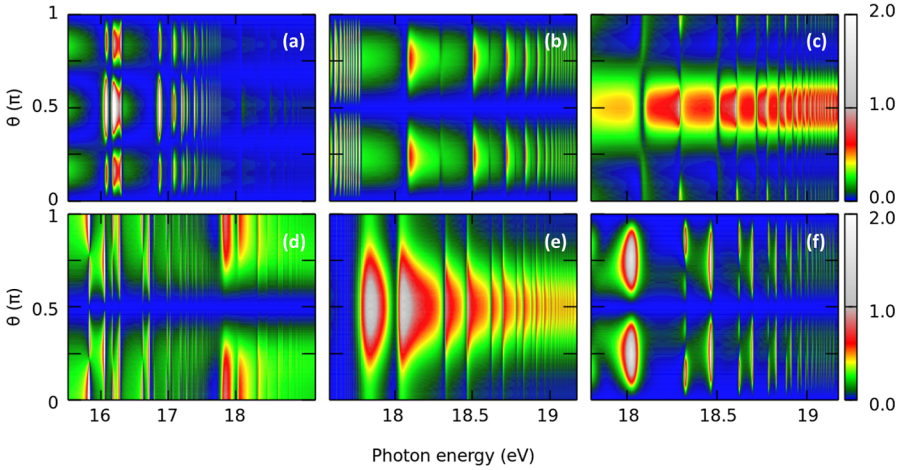


Figure 7. Molecular frame photoelectron angular distributions, at a fixed azimuthal angle ϕ, as a function of the photon energy. Top row: Molecular axis is placed parallel to the light polarization vector, with $\phi = 0$, for the channels (a) $X^2\Pi_g$, (b) $A^2\Pi_u$, and (c) $B^2\Sigma_u^+$. Bottom row: Molecular axis is placed perpendicular to the light polarization vector, with $\phi = \pi/2$, for the channels (d) $X^2\Pi_g$, (e) $A^2\Pi_u$, and (f) $B^2\Sigma_u^+$. Results have been normalized by a constant factor for a better visualization.

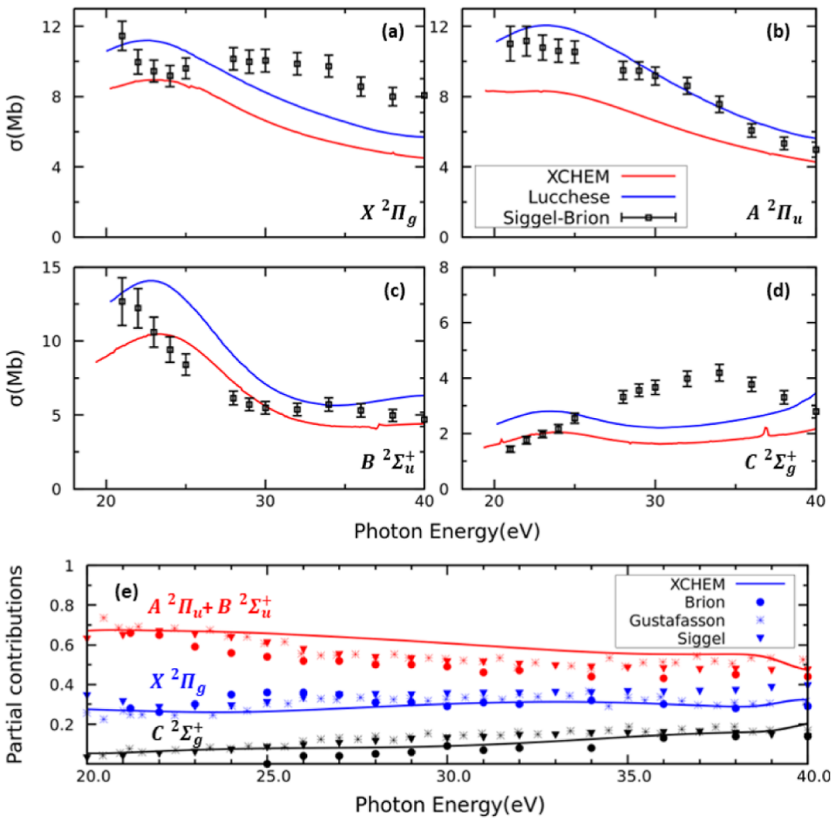


Figure 8. (a) Total cross section for single-photon ionization as a function of the photon energy. Panels (a)−(d) depict the cross section correlated to each ionization channel (see insets). Black points: Experimental results from refs 34 and 37. Solid blue line: Theoretical from ref 40. (e) Branching ratios for various ionization channels compared with the experimental results from refs 34, 35, and 37.

these calculations). However, most of the series identified here have been previously observed, although not characterized, experimentally.

We have also evaluated molecular-frame photoelectron angular distribution, i.e., cross sections resolved in molecular orientation and photoelectron emission angle with respect to the polarization direction, with particular emphasis on the range of photon energies between the first and fourth ionization thresholds. As we have seen, this energy region features multiple series of autoionizing Rydberg states. The MFPAD is very sensitive to electron correlation in the vicinity of autoionizing states and thus requires a fully correlated treatment of both the target electronic states and the electronic continuum. Figure 7a−c depicts the MFPADs for photoionization from the ground state leading to states of $^1\Sigma_u^+$ symmetry, i.e., the molecular axis is placed parallel to the light polarization vector, as a function of the photon energy. Each panel presents the MFPADs at a fixed azimuthal angle $\phi = 0$

https://doi.org/10.1021/acs.jpca.3c06947
J. Phys. Chem. A 2024, 128, 182−190

associated with the $X^2\Pi_g$, $A^2\Pi_u$, and $B^2\Sigma_u^+$ cation states, respectively. Figure 7d–f depicts the corresponding MFPADs at a fixed azimuthal angle $\phi = \pi/2$ for photoionization from the ground state leading to states of $^1\Pi_u$ symmetry, i.e., the molecular axis is placed perpendicular to the light polarization vector. In general, for a given ionization channel, the off-resonance MFPADs exhibit a smooth behavior as a function of photon energy. The photoelectrons are mainly ejected in a preferential direction for all photon energies. In contrast, in the vicinity of a resonance, the MFPADs experience strong variations as the photon energy crosses their energy position. This effect is a direct consequence of the sudden change in the phase of the scattering state describing the photoelectron at resonance. This change in the phase modifies the ratio between the partial cross sections. This ultimately leads to a different dominant partial wave and thus to an abrupt change in the MFPADs. This effect has been extensively studied in both atomic and molecular systems.[20,21,57,58] As observed in Figure 7c, the off-resonance photoelectron is primarily emitted at 90°. However, the on-resonance photoelectrons are mainly ejected at 0 and 180°. Examination of the partial cross sections (not shown here) suggests that the $\varepsilon s + \varepsilon d$ and the $\varepsilon s + \varepsilon g$ channels dominate in the vicinity of the $4\sigma_g^{-1}np\sigma_u$ and $4\sigma_g^{-1}nf\sigma_u$ resonances, respectively, while the εs channel becomes the prominent channel elsewhere. A similar analysis can be made for the different ionization channels, although the presence of overlapping resonances makes the interpretation more difficult.

Finally, for the sake of completeness, Figure 8a–d shows the total cross sections associated with leaving the cation in each of the four included channels for photon energies 20 eV $\leq \hbar\omega \leq$ 40 eV. This energy region has been extensively studied both theoretically and experimentally.[34−42] The present results are compared with experimental data obtained using synchrotron radiation measurements[34−38] and theoretical results calculated using Hartree–Fock static-exchange potentials.[40] The corresponding β asymmetry parameters are presented in Figure 9a–d. The cross sections and the β asymmetry parameters are generally in good agreement with the experimental data, in particular for the $X^2\Pi_g$, $A^2\Pi_u$, and $B^2\Sigma_u^+$ cation states. In contrast, the cross section for the $C^2\Sigma_g^+$ cation state deviates somewhat from the experimental data. Although the present calculations do not include averaging over the vibrational motion of the molecule, previous calculations seem to indicate that the inclusion of the effects of the nuclear motion would not alter considerably the cross sections in this energy region.[39,41] On the other hand, calculations reported in ref 42 including up to 96 channels in the close-coupling expansion exhibit a very good agreement with the experiment in this energy region. Therefore, the reason for the present discrepancy in the $C^2\Sigma_g^+$ channel is the lack of higher ionization channels in the close-coupling expansion. For completeness, the cross section branching ratios associated with the $X^2\Pi_g$, $A^2\Pi_u$ + $B^2\Sigma_u^+$, and $C^2\Sigma_g^+$ states are presented in Figure 8e. The agreement between experiment and theory is excellent, despite the discrepancy found for the $C^2\Sigma_g^+$ state cross section. As observed, photoionization in this energy region leads mainly to the $X^2\Pi_g$, $A^2\Pi_u$, and $B^2\Sigma_u^+$ cation states with similar probabilities. In contrast, the population of the $C^2\Sigma_g^+$ state only becomes significant for photon energies higher than 30 eV.

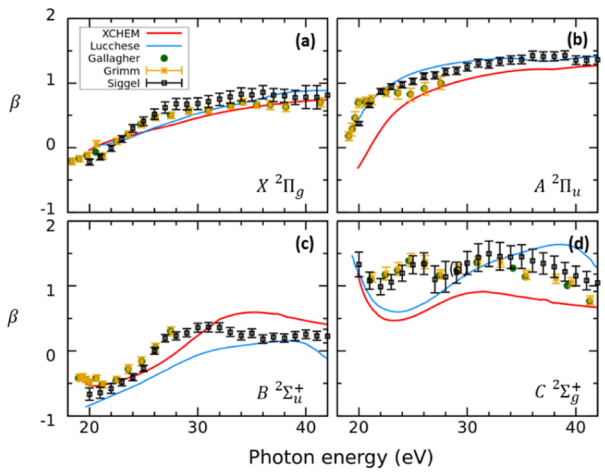


Figure 9. Photoelectron angular distribution asymmetry parameter β for single-photon ionization as a function of the photon energy. Each panel depicts the β parameter correlated to each ionization channel (see insets). Yellow asterisks, green dots, and black squares are experimental results from refs 36 and 38 and, ref 37, respectively. Blue dots: theoretical results from ref 40. Red line: Presents results.

CONCLUSIONS

Valence-shell single-photon ionization of the CO_2 molecule has been theoretically studied by using the XCHEM methodology. This method makes use of a fully correlated electronic continuum and can therefore provide an accurate description of photoionization processes in the presence of Rydberg autoionizing states. We have evaluated the fully differential photoionization cross sections, with particular interest in the range of photon energies between the first and fourth ionization thresholds. This energy region features multiple series of autoionizing Rydberg states. The members of the different series have been assigned and their corresponding energy positions, autoionization widths, and quantum defects have been reported. While some of these Rydberg series have been previously observed experimentally, no theoretical description of them has been given. These results illustrate the significance of using highly correlated methods when describing photoionization processes of many-electron systems. The present calculations provide a benchmark for future attosecond pump–probe experiments in CO_2, specifically those aiming to study the energy region between the first and fourth ionization thresholds.

AUTHOR INFORMATION

Corresponding Author

Roger Y. Bello – *Departamento de Química Física Aplicada, Universidad Autónoma de Madrid, 28049 Madrid, Spain;* orcid.org/0000-0001-9576-6479; Email: roger.bello@uam.es

Authors

Prateek Pranjal – *Instituto Madrileño de Estudios Avanzados en Nanociencia (IMDEA-Nanociencia), Cantoblanco, 28049 Madrid, Spain;* orcid.org/0000-0003-2050-0945

Jesús González-Vázquez – *Departamento de Química, Módulo 13, Facultad de Ciencias, Universidad Autónoma de Madrid, 28049 Madrid, Spain;* orcid.org/0000-0003-2204-3549

Fernando Martín – *Instituto Madrileño de Estudios Avanzados en Nanociencia (IMDEA-Nanociencia), Cantoblanco, 28049 Madrid, Spain; Departamento de*

https://doi.org/10.1021/acs.jpca.3c06947
J. Phys. Chem. A 2024, 128, 182–190

Química, Módulo 13, Facultad de Ciencias, Universidad Autónoma de Madrid, 28049 Madrid, Spain; orcid.org/0000-0002-7529-925X

Complete contact information is available at: https://pubs.acs.org/10.1021/acs.jpca.3c06947

Notes

The authors declare no competing financial interest.

■ ACKNOWLEDGMENTS

All calculations were performed at the Mare Nostrum Supercomputer of the Red Española de Supercomputación (BSC-RES) and the Centro de Computación Científica de la Universidad Autónoma de Madrid (CCC-UAM). Work supported by the Synergy Grant of the European Research Council TOMATTO (ref 951224), the projects PDC2021-121073-I00, PID2019-105458RB-I00, and PID2019-106732GB-I00 funded by MCIN/AEI/10.13039/501100011033 and by the European Union "NextGenerationEU"/PRTRMICINN programs, and the "Severo Ochoa" Programme for Centres of Excellence in R&D (CEX2020-001039-S).

■ REFERENCES

(1) Sansone, G.; Kelkensberg, F.; Perez-Torres, J. F.; Morales, F.; Kling, M. F.; Siu, W.; Ghafur, O.; Johnsson, P.; Swoboda, M.; Benedetti, E.; et al. Electron Localization Following Attosecond Molecular Photoionization. *Nature* **2010**, *465*, 763−766.

(2) Calegari, F.; Ayuso, D.; Trabattoni, A.; Belshaw, L.; De Camillis, S.; Anumula, S.; Frassetto, F.; Poletto, L.; Palacios, A.; Decleva, P.; et al. Ultrafast Electron Dynamics in Phenylalanine Initiated by Attosecond Pulses. *Science* **2014**, *346*, 336−339.

(3) Kelkensberg, F.; Siu, W.; Pérez-Torres, J. F.; Morales, F.; Gademann, G.; Rouzée, A.; Johnsson, P.; Lucchini, M.; Calegari, F.; Sanz-Vicario, J. L.; et al. Attosecond Control in Photoionization of Hydrogen Molecules. *Phys. Rev. Lett.* **2011**, *107*, 043002.

(4) Trabattoni, A.; Klinker, M.; González-Vázquez, J.; Liu, C.; Sansone, G.; Linguerri, R.; Hochlaf, M.; Klei, J.; Vrakking, M. J. J.; Martín, F.; et al. Mapping the Dissociative Ionization Dynamics of Molecular Nitrogen with Attosecond Time Resolution. *Phys. Rev. X* **2015**, *5*, 041053.

(5) Eckstein, M.; Yang, C.-H.; Frassetto, F.; Poletto, L.; Sansone, G.; Vrakking, M. J. J.; Kornilov, O. Direct Imaging of Transient Fano Resonances in N_2 Using Time-Energy-and Angular-Resolved Photoelectron Spectroscopy. *Phys. Rev. Lett.* **2016**, *116*, 163003.

(6) Nisoli, M.; Decleva, P.; Calegari, F.; Palacios, A.; Martín, F. Attosecond Electron Dynamics in Molecules. *Chem. Rev.* **2017**, *117*, 10760−10825.

(7) Huppert, M.; Jordan, I.; Baykusheva, D.; von Conta, A.; Wörner, H. J. Attosecond Delays in Molecular Photoionization. *Phys. Rev. Lett.* **2016**, *117*, 093001.

(8) Cattaneo, L.; Vos, J.; Bello, R. Y.; Palacios, A.; Heuser, S.; Pedrelli, L.; Lucchini, M.; Cirelli, C.; Martín, F.; Keller, U. Attosecond coupled electron and nuclear dynamics in dissociative ionization of H2. *Nat. Phys.* **2018**, *14*, 733−738.

(9) Lara-Astiaso, M.; Galli, M.; Trabattoni, A.; Palacios, A.; Ayuso, D.; Frassetto, F.; Poletto, L.; De Camillis, S.; Greenwood, J.; Decleva, P.; et al. Attosecond Pump−Probe Spectroscopy of Charge Dynamics in Tryptophan. *J. Phys. Chem. Lett.* **2018**, *9*, 4570−4577.

(10) Cattaneo, L.; Pedrelli, L.; Bello, R. Y.; Palacios, A.; Keathley, P. D.; Martín, F.; Keller, U. Isolating Attosecond Electron Dynamics in Molecules where Nuclei Move Fast. *Phys. Rev. Lett.* **2022**, *128*, 063001.

(11) Månsson, E. P.; Latini, S.; Covito, F.; Wanie, V.; Galli, M.; Perfetto, E.; Stefanucci, G.; Hübener, H.; De Giovannini, U.; Castrovilli, M. C.; et al. Real-time observation of a correlation-driven sub 3 fs charge migration in ionised adenine. *Commun. Chem.* **2021**, *4*, 73.

(12) Calegari, F.; Martin, F. Open questions in attochemistry. *Commun. Chem.* **2023**, *6*, 184.

(13) Glownia, J. M.; Natan, A.; Cryan, J. P.; Hartsock, R.; Kozina, M.; Minitti, M. P.; Nelson, S.; Robinson, J.; Sato, T.; van Driel, T.; et al. Self-Referenced Coherent Diffraction X-Ray Movie of Ångstrom- and Femtosecond-Scale Atomic Motion. *Phys. Rev. Lett.* **2016**, *117*, 153003.

(14) Poullain, S. M.; Kobayashi, Y.; Chang, K. F.; Leone, S. R. Visualizing coherent vibrational motion in the molecular iodine $B\ ^3\Pi_{0^+_u}$ state using ultrafast XUV transient-absorption spectroscopy. *Phys. Rev. A* **2021**, *104*, 022817.

(15) Gruson, V.; Barreau, L.; Jiménez-Galan, Á.; Risoud, F.; Caillat, J.; Maquet, A.; Carré, B.; Lepetit, F.; Hergott, J.-F.; Ruchon, T.; et al. Attosecond dynamics through a Fano resonance: Monitoring the birth of a photoelectron. *Science* **2016**, *354*, 734−738.

(16) Haessler, S.; Fabre, B.; Higuet, J.; Caillat, J.; Ruchon, T.; Breger, P.; Carré, B.; Constant, E.; Maquet, A.; Mével, E.; et al. Phase-Resolved Attosecond Near-Threshold Photoionization of Molecular Nitrogen. *Phys. Rev. A* **2009**, *80*, 011404.

(17) Nandi, S.; Plésiat, E.; Zhong, S.; Palacios, A.; Busto, D.; Isinger, M.; Neoričić, L.; Arnold, C. L.; Squibb, R. J.; Feifel, R.; et al. Attosecond timing of electron emission from a molecular shape resonance. *Sci. Adv.* **2020**, *6*, No. eaba7762.

(18) Ahmadi, H.; Plésiat, E.; Moioli, M.; Frassetto, F.; Poletto, L.; Decleva, P.; Schröter, C. D.; Pfeifer, T.; Moshammer, R.; Palacios, A.; et al. Attosecond photoionisation time delays reveal the anisotropy of the molecular potential in the recoil frame. *Nat. Commun.* **2022**, *13*, 1242.

(19) Borràs, V. J.; González-Vázquez, J.; Argenti, L.; Martín, F. Attosecond photoionization delays in the vicinity of molecular Feshbach resonances. *Sci. Adv.* **2023**, *9*, No. eade3855.

(20) Stratmann, R. E.; Lucchese, R. R. A graphical unitary group approach to study multiplet specific multichannel electron correlation effects in the photoionization of O2. *J. Chem. Phys.* **1995**, *102*, 8493−8505.

(21) Stratmann, R. E.; Zurales, R. W.; Lucchese, R. R. Multiplet-specific multichannel electron-correlation effects in the photoionization of NO. *J. Chem. Phys.* **1996**, *104*, 8989−9000.

(22) Bello, R. Y.; Lucchese, R. R.; Rescigno, T. N.; McCurdy, C. W. Correlated variational treatment of ionization coupled to nuclear motion: Ultrafast pump and ionizing probe of electronic and nuclear dynamics in LiH. *Phys. Rev. Res.* **2021**, *3*, 013228.

(23) Schneider, B. I.; Rescigno, T. N. Complex Kohn variational method: Application to low-energy electron-molecule collisions. *Phys. Rev. A* **1988**, *37*, 3749−3754.

(24) McCurdy, C. W.; Rescigno, T. N. Collisions of electrons with polyatomic molecules: Electron-methane scattering by the complex Kohn variational method. *Phys. Rev. A* **1989**, *39*, 4487−4493.

(25) Carr, J. M.; Galiatsatos, P. G.; Gorfinkiel, J. D.; Harvey, A. G.; Lysaght, M. A.; Madden, D.; Mašín, Z.; Plummer, M.; Tennyson, J.; Varambhia, H. N. UKRmol: a low-energy electron- and positron-molecule scattering suite. *Eur. Phys. J. D* **2012**, *66*, 58.

(26) Marante, C.; Argenti, L.; Martín, F. Hybrid Gaussian−B-spline basis for the electronic continuum: Photoionization of atomic hydrogen. *Phys. Rev. A* **2014**, *90*, 012506.

(27) Marante, C.; Klinker, M.; Corral, I.; González-Vázquez, J.; Argenti, L.; Martín, F. Hybrid-basis close-coupling interface to quantum chemistry packages for the treatment of ionization problems. *J. Chem. Theory Comput.* **2017**, *13*, 499−514.

(28) Marante, C.; Klinker, M.; Kjellsson, T.; Lindroth, E.; González-Vázquez, J.; Argenti, L.; Martín, F. Photoionization using the xchem approach: Total and partial cross sections of Ne and resonance parameters above the $2s^22p^5$ threshold. *Phys. Rev. A* **2017**, *96*, 022507.

(29) Bello, R. Y.; Borràs, V. J.; González-Vázquez, J.; Martín, F. Electronic coherences in argon through interfering one-and two-photon ionization processes in the vicinity of Feshbach resonances. *Phys. Rev. Res.* **2022**, *4*, 043028.

(30) Klinker, M.; Marante, C.; Argenti, L.; González-Vázquez, J.; Martín, F. Electron correlation in the ionization continuum of molecules: photoionization of N2 in the vicinity of the hopfield series of autoionizing states. *J. Phys. Chem. Lett.* **2018**, *9*, 756−762.
(31) Klinker, M.; Marante, C.; Argenti, L.; González-Vázquez, J.; Martín, F. Partial cross sections and interfering resonances in photoionization of molecular nitrogen. *Phys. Rev. A* **2018**, *98*, 033413.
(32) Marggi Poullain, S.; Klinker, M.; González-Vázquez, J.; Martín, F. Resonant photoionization of O_2 up to the fourth ionization threshold. *Phys. Chem. Chem. Phys.* **2019**, *21*, 16497−16504.
(33) Fernández-Milán, P.; Borràs, V. J.; González-Vázquez, J.; Martín, F. Photoionization of the water molecule with XCHEM. *J. Chem. Phys.* **2023**, *158*, 134305.
(34) Brion, C.; Tan, K. Partial oscillator strengths for the photoionization of N2O and CO_2 (20−60 eV). *Chem. Phys.* **1978**, *34*, 141−151.
(35) Gustafsson, T.; Plummer, E.; Eastman, D.; Gudat, W. Partial photoionization cross sections of CO_2 between 20 and 40 eV studied with synchrotron radiation. *Phys. Rev. A* **1978**, *17*, 175−181.
(36) Gallagher, J.; Brion, C.; Samson, J.; Langhoff, P. Absolute cross sections for molecular photoabsorption, partial photoionization, and ionic photofragmentation processes. *J. Phys. Chem. Ref. Data* **1988**, *17*, 9−153.
(37) Siggel, M.; West, J.; Hayes, M.; Parr, A. C.; Dehmer, J. L.; Iga, I. Shape-resonance-enhanced continuum−continuum coupling in photoionization of CO_2. *J. Chem. Phys.* **1993**, *99*, 1556−1563.
(38) Grimm, F. A.; Allen, J. D.; Carlson, T. A.; Krause, M. O.; Mehaffy, D.; Keller, P. R.; Taylor, J. W. Angle-resolved photoelectron spectroscopy of CO_2 with synchrotron radiation. *J. Chem. Phys.* **1981**, *75*, 92−98.
(39) Lucchese, R. R.; McKoy, V. Vibrational effects in the photoionization shape resonance leading to the C2Σg+state of C O2+. *Phys. Rev. A* **1982**, *26*, 1992−1996.
(40) Lucchese, R. R. Effects of interchannel coupling on the photoionization cross sections of carbon dioxide. *J. Chem. Phys.* **1990**, *92*, 4203−4211.
(41) Yu, C. H.; Pitzer, R. M.; McCurdy, C. W. Effect of vibration on photoionization of carbon dioxide in the $4\sigma_g$ channel. *J. Phys. Chem.* **1988**, *92*, 3116−3122.
(42) Harvey, A. G.; Brambila, D. S.; Morales, F.; Smirnova, O. An R-matrix approach to electron−photon−molecule collisions: photoelectron angular distributions from aligned molecules. *J. Phys. B: At., Mol. Opt. Phys.* **2014**, *47*, 215005.
(43) Wang, L.-S.; Reutt, J.; Lee, Y.-T.; Shirley, D. High resolution UV photoelectron spectroscopy of CO+2, COS+ and CS+2 using supersonic molecular beams. *J. Electron Spectrosc. Relat. Phenom.* **1988**, *47*, 167−186.
(44) Tanaka, Y.; Jursa, A.; LeBlanc, F. Higher ionization potentials of linear triatomic molecules. I. CO_2. *J. Chem. Phys.* **1960**, *32*, 1199−1205.
(45) Tanaka, Y.; Ogawa, M. Rydberg absorption series of CO_2 converging to the 2Πu state of CO2+. *Can. J. Phys.* **1962**, *40*, 879−886.
(46) Henning, H. J. Die Absorptionsspektren von Kohlendioxyd, Kohlenmonoxyd und Wasserdampf im Gebiet von 600−900 ÅE. *Ann. Phys.* **1932**, *405*, 599−620.
(47) Parr, A. C.; Dehmer, P. M.; Dehmer, J. L.; Ueda, K.; West, J.; Siggel, M.; Hayes, M. Selective population of spin−orbit levels in the autoionization of a polyatomic molecule: Branching ratios and asymmetry parameters for the Tanaka−Ogawa Rydberg series in CO_2. *J. Chem. Phys.* **1994**, *100*, 8768−8779.
(48) Shaw, D.; Holland, D.; Hayes, M.; MacDonald, M.; Hopkirk, A.; McSweeney, S. A study of the absolute photoabsorption, photoionisation and photodissociation cross sections and the photoionisation quantum efficiency of carbon dioxide from the ionisation threshold to 345 Å. *Chem. Phys.* **1995**, *198*, 381−396.
(49) Fridh, C.; Åsbrink, L.; Lindholm, E. Valence excitation of linear molecules. II. Excitation and UV spectra of C_2N_2, CO_2 and N_2O. *Chem. Phys.* **1978**, *27*, 169−181.
(50) Furch, F. J.; Birkner, S.; Jungmann, J. H.; Kelkensberg, F.; Schulz, C. P.; Rouzée, A.; Vrakking, M. J. Photoelectron imaging of XUV photoionization of CO_2 by 13−40 eV synchrotron radiation. *J. Chem. Phys.* **2013**, *139*, 124309.
(51) Aquilante, F.; Autschbach, J.; Carlson, R. K.; Chibotaru, L. F.; Delcey, M. G.; De Vico, L.; Fdez Galván, I.; Ferré, N.; Frutos, L. M.; Gagliardi, L.; et al. Molcas 8: New capabilities for multiconfigurational quantum chemical calculations across the periodic table. *J. Comput. Chem.* **2016**, *37*, 506.
(52) Kendall, R. A.; Dunning, T. H.; Harrison, R. J., Jr. Electron affinities of the first-row atoms revisited. Systematic basis sets and wave functions. *J. Chem. Phys.* **1992**, *96*, 6796−6806.
(53) Benda, J.; Mašín, Z.; Gorfinkiel, J. D. Analysis of RABITT time delays using the stationary multiphoton molecular R-matrix approach. *Phys. Rev. A* **2022**, *105*, 053101.
(54) Kelkensberg, F.; Rouzée, A.; Siu, W.; Gademann, G.; Johnsson, P.; Lucchini, M.; Lucchese, R.; Vrakking, M. XUV ionization of aligned molecules. *Phys. Rev. A* **2011**, *84*, 051404.
(55) Hazi, A. U. Behavior of the eigenphase sum near a resonance. *Phys. Rev. A* **1979**, *19*, 920−922.
(56) Shaw, D.; Holland, D.; Hayes, M.; MacDonald, M.; Hopkirk, A.; McSweeney, S. A study of the absolute photoabsorption, photoionisation and photodissociation cross sections and the photoionisation quantum efficiency of carbon dioxide from the ionisation threshold to 345 Å. *Chem. Phys.* **1995**, *198*, 381−396.
(57) Berrah, N.; Langer, B.; Bozek, J.; Gorczyca, T. W.; Hemmers, O.; Lindle, D. W.; Toader, O. Angular-distribution parameters andR-matrix calculations of Ar resonances. *J. Phys. B: At., Mol. Opt. Phys.* **1996**, *29*, 5351−5365.
(58) Lebech, M.; Houver, J. C.; Dowek, D.; Lucchese, R. R. Molecular Frame Photoelectron Emission in the Presence of Autoionizing Resonances. *Phys. Rev. Lett.* **2006**, *96*, 073001.

https://doi.org/10.1021/acs.jpca.3c06947
J. Phys. Chem. A 2024, 128, 182−190